Available online at www.sciencedirect.com
ScienceDirect
Journal of the European Ceramic Society 29 (2009) 919–924
www.elsevier.com/locate/jeurceramsoc

Optical characterization of stereolithography alumina suspensions using the Kubelka–Munk model

Y. Abouliatim [a,b,*], T. Chartier [a], P. Abelard [a], C. Chaput [b], C. Delage [b]

[a] SPCTS, UMR CNRS 6638, ENSCI, 47/73 Avenue Albert Thomas, 87065 Limoges, France
[b] CTTC, Parc d'Ester Technopole, Rue Soyouz, BP36823, 87068 Limoges, France

Available online 3 January 2009

Abstract

The multiple light scattering in concentrated alumina suspensions adapted to stereolithography can be modeled using diffuse reflectance measurements coupled to the Kubelka–Munk model. The penetration depth of UV radiation can be related to the scattering coefficient allowing the prediction of the cure depth with an accuracy of 20%.

Keywords: Stereolithography; Scattering; Alumina; Kubelka–Munk

1. Introduction

Ceramic stereolithography is a rapid prototype technique allowing elaboration of 3-D complex architectures, without tooling or machining, directly from a computer aided design (CAD) file. The fabrication of green parts is performed by scanning an UV laser beam (351 nm) on a curable system containing non absorbing ceramic particles. Curing is performed line-by-line and layer-by-layer sequences.

Developed first[1] for polymeric materials, the stereolithography was extended to freeform ceramics parts by introducing ceramics particles in the UV curable system.[2] Several formulations containing at least 40 vol.% of ceramic powder have been developed to ensure (i) an adequate rheological behavior for spreading homogenous thin layers, (ii) to be reactive to UV and, (iii) to lead dense parts after heat treatment.[3–13]

However, the introduction of ceramic particles in monomer reactive systems increases a level of complexity due to multiple scattering phenomena witch reduces the cure depth and thereafter increases the processing time and dimensional resolution.

For unloaded stereolithography systems, the interaction between UV radiation and photo-polymeric resin can be described by Beer's law:

$$E = E_i \exp(-\alpha z) \tag{1}$$

where the density of energy E (mJ/cm^2) is related to depth z through the extinction coefficient α. E_i is the density of energy of the incident light. In this case, the cure depth C_D is the distance required to attenuate E to the threshold energy density E_C (mJ/cm^2) required for photopoly-mérisation. It's expressed by:

$$C_D = \frac{1}{\alpha} \ln\left(\frac{E_i}{E_c}\right) \tag{2}$$

Similarly, for a loaded stereolithography system, the cure depth is related to the laser density and the threshold energy density via the Jacobs equation derived from the Beer's law:

$$C_D = D_p \ln\left(\frac{E_i}{E_c}\right) \tag{3}$$

where D_p is the resin sensitivity or depth of penetration, distance at which the laser intensity is reduced by e^{-1}.

D_p is a critical parameter in stereolithography. D_p illustrates the divergence from the homogeneous case (unloaded systems) and takes into account scattering phenomena that control the cure depth in the case of the turbid suspensions (loaded systems).

Since the extension of stereolithography to the fabrication of ceramics parts, the D_p parameter has been investigated by several authors.[5,13,14]

Griffith and Halloran[5] related this parameter to the square of the refractive index difference between the ceramic particles and the medium ($\Delta n^2 = (n_p - n_0)^2$), to the interparticle spacing

* Corresponding author. Tel.: +33 5 55 45 22 25; fax: +33 5 55 79 69 54.
E-mail address: thierry.chartier@unilim.fr (T. Chartier).

0955-2219/$ – see front matter © 2008 Elsevier Ltd. All rights reserved.
doi:10.1016/j.jeurceramsoc.2008.07.008

(s) and to the UV wavelength (λ) via the expression:

$$D_p \propto \frac{2d_{50}}{3}\frac{\lambda}{s}\frac{n_0}{\Delta n^2} \quad (4)$$

where d_{50} is the average particle size.

More recently, Wu et al.[13] related the depth of penetration to the photon transport mean free path (l*):

$$\frac{1}{D_p(1-\Phi)c_{PI}} \approx A\frac{1}{l^*(1-\Phi)c_{PI}} + \alpha_{PI} \quad (5)$$

where A is an empirical constant, ϕ the powder volume fraction, α_{PI} the molar absorptivity ($M^{-1}\,\mu m^{-1}$) of the UV photoinitiator and c_{PI} the photoinitiator concentration.

Both these expressions are in good agreement with measured values of D_p and can be used to optimize stereolithography suspensions and/or to predict the cure depth. But they require the knowledge of the physical and optical properties of the various components of the ceramic suspensions which are not easy to obtain (refractive index of mixed powders, interparticle spacing in the case of randomly distributed non spherical particles. . .)

This paper deals with the evaluation of the D_p parameter using a two-flux continuum model, called Kubelka–Munk (K-M) model.[15–17]

2. Experimental procedures

Three α-alumina powders, with different mean particle size (P152, P152SB and P172B, Alcan-Péchiney, France) are used. As-received alumina powders were attrition-milled for deagglo-meration. The millings were performed in ethanol containing 1 wt.% of an electrosteric dispersant (CP213, Cerampilot, France), with respect to the powder. Three narrower particle size distributions were obtained (Fig. 1).

The UV curable system consists of a photoinitiator (Irgacure 651, Ciba, Switzerland) absorbing in the range of the UV laser emission (Ar-ion laser, coherent, (= 351–364 nm) and a low viscosity photopolymerisable monomer (M) with a refractive index of 1.50.

Suspensions of various loading (1–55 vol.%) were prepared by first, dissolving the photoinitiator (0.5 wt.% on monomer basis) in the monomer, mixing for 24 h, adding the ceramic powder and then mixing/milling during 20 min with a three roll mills to break down the agglomerates and to achieve a good homogeneity.

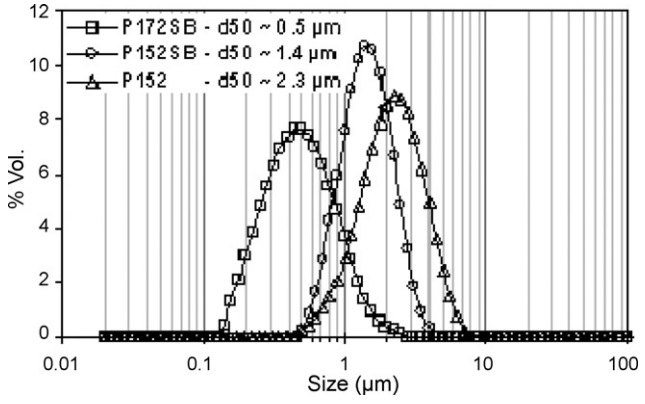

Fig. 1. Particle size distribution of alumina powders after attrition milling (Mastersizer 2000 particle size analyzer; Malvern, England).

The curing properties of the suspensions were studied using one SLA machine (Optoform, France). One-layer parts (windowpanes) of $10 \times 40\,mm^2$ were drawn by one scanning of the laser beam at variable energy density. Pitches of 1 mm were chosen in order to recover the windowpane in an independent polymerized features structure. After exposure, polymerized samples were removed from the uncured paste and cleaned. Then, profile, cure depth and cure width were observed and measured by optical microscopy (Eclipse 50 i, Nikon, Japan).

The optical properties (diffuse reflectance and transmittance measurements) of the alumina suspensions were inspected in the range of 300–400 nm using an UV-vis light spectrophotometer (Lambda 40, PerkinElmer, USA) equipped with a 51 mm diameter integrating sphere accessory (RSA-PE-20, Labsphere, Inc., USA). During diffuse reflectance measurements, a totally reflecting ($R = 100\%$) standard white (Spectralon, Labsphere, Inc., USA) and a thick absorbing black SiC plate ($e_{SiC} = 1.5$ cm, $A = 95\%$) were used as white or black background, respectively.

The K-M model assumes diffuse illumination and enables the calculation of the absorption (K) and scattering (S) from diffuse spectral measurements. But, this model does not take into account the multiple reflections at the surface due to the refractive index discontinuities at the air/layer interface. Then, spectral measurements need to be corrected before applying the model, using for instance the Saunderson's correction.[18] This correction requires the determination of the external and internal correcting coefficients in order to correct the fraction of the light reflected both from the air/layer interface and from the layer/air interface due to the light reflected from the back surface of the sample.[6,19] Different values of these coefficients are available in the literature,[19–22] computing on the basis of an estimated mean refractive index of turbid suspensions (principally dental resins reinforced by ceramic or glass particles), but doesn't take into account the variation of powder concentration. In this respect, we have chosen, in a first approach, to use the K-M model without corrections.

In order to decrease the interfaces phenomena, due to the change of the index of refraction, we have measured the optical properties of free thin layer without sample cavity. However, the measure of transmittance of high loaded suspension (>35 vol.%) imposes a small thickness film (<150 μm). Then, 50 μm thick layers were performed by tape casting the suspension on a highly UV-transmitting film, ($e_{film} = 50$ μm, $T \sim 90\%$ at $\lambda = 351$ nm) (SP: silicone polyester, Isolant-Sudouest, France). Actually, these optical measurements (transmission, reflection and absorption) are those of the bi-layers (50/50 μm) ceramic suspension/silicone polyester. However, the coefficient K and S determined by the diffuse reflectance measurement and the K-M model are intrinsic to the 50 μm ceramic suspension layer while the SP film was included in the background (white backing = film SP + Spectralon; black backing = film SP + SiC plate).

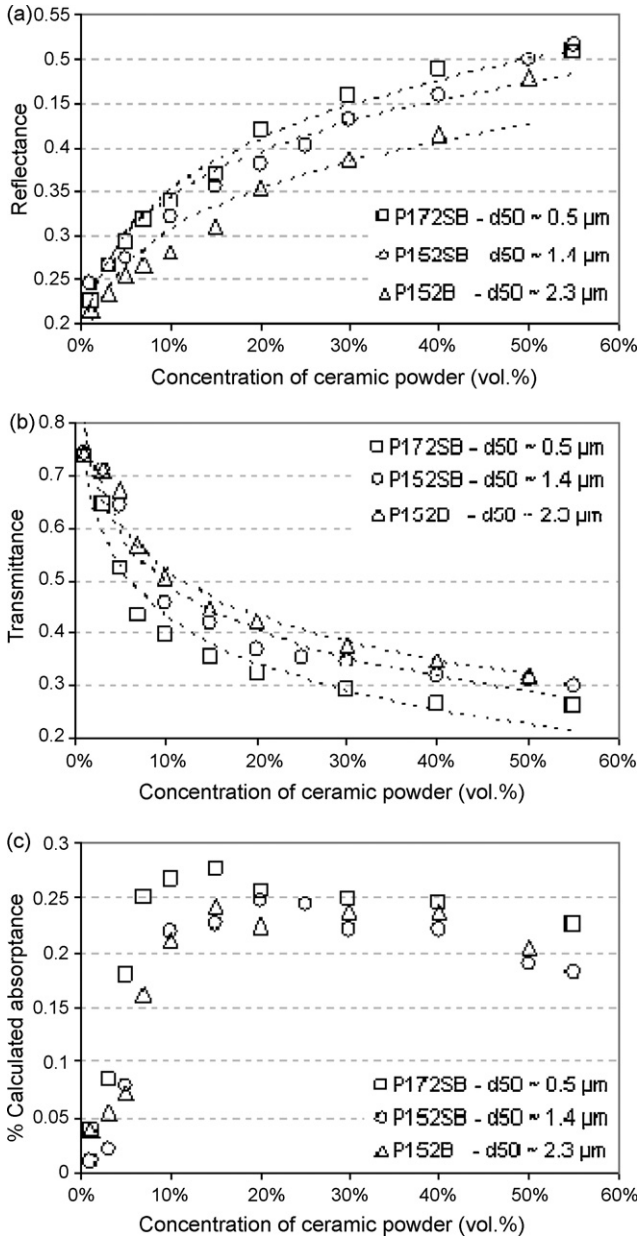

Fig. 2. Variation of the UV transmittance (a), reflectance (b) and calculated absorptance (c) of the bi-layer ceramic suspensions/SP for different concentrations of the three alumina used at $\lambda = 351$ nm.

3. Results and discussion

3.1. Optical characterization of alumina suspensions

As expected, for the three alumina powders, the diffuse reflectance is increasing, and the transmittance is decreasing, with the powder loading (Fig. 2a and b).

In addition, the diffuse reflectance is decreasing and the diffuse transmittance is increasing with the increase of the mean particle size. That can be likely attributed to the diminution of the total scattering due to the reduction of the number of the scattering centers. The absorptance, calculated as $(1 - R - T)$, is increasing with the powder concentration until a maximum reached between 10 and 20 vol.%, then is slightly decreasing for larger powder loading (Fig. 2c).

The explanation may lie in the variation of the length of the light trajectory with the powder loading, which has been schematized in Fig. 3. Path lengths of the light in the sample are extended by the presence of ceramic particles due to the scattering (Fig. 3a and b). Interactions with the reactive monomer, then adsorption, are increasing with the path length. The maximum of absorption, obtained for 10–20 vol.% powder, suggests that the corresponding arrangement of particles allows the light to have a maximum trajectory length in the monomer absorbent medium (Fig. 3b). Beyond this maximum powder concentration, the multiple scattering phenomena becomes predominant thus, decreasing the path length and minimize interactions with the reactive monomer (Fig. 3c).

3.2. Computation of S and K coefficients by the K-M analysis

The expressions allowing the calculation of K and S from reflectance measurements over two backgrounds are:[19]

$$K = \frac{Z}{D}\left(\frac{1 - R_\infty}{1 + R_\infty}\right); \qquad S = \frac{Z}{D}\left(\frac{2R_\infty}{1 + R_\infty^2}\right) \tag{6}$$

where R_∞ is the reflectance of an opaque layer, as defined by K-M theory, Z and D are respectively the optical and the physical thickness of the layer. R_∞ and Z are calculated from measured reflections over the two different backgrounds (highly absorbent black one and totally reflecting white one) as:

$$R_\infty = B - (B^2 - 1)^{1/2} \tag{7}$$

with:

$$B = \frac{(1+R_\mathrm{b}R_\mathrm{w})(R_\mathrm{g,w}-R_\mathrm{g,b}) - (1 + R_\mathrm{g,b}R_\mathrm{g,w})(R_\mathrm{w} - R_\mathrm{b})}{2(R_\mathrm{b}R_\mathrm{g,w} - R_\mathrm{g,b}R_\mathrm{w})} \tag{8}$$

where R_w and R_b are respectively the reflectance of the sample over white and black backing. $R_\mathrm{g,w}$ and $R_\mathrm{g,b}$ are respectively the reflectance of the white and black backgrounds and

$$Z = \tfrac{1}{2}\ln(\beta + 1)$$

where:

$$\beta = \left(\frac{R_\mathrm{g,b} - R_\mathrm{b}}{R_\mathrm{b} - R_\infty}\right)\left(\frac{1 - R_\infty^2}{1 - R_\mathrm{g,b}R_\infty}\right) \tag{9}$$

The variations of S and K coefficients are in agreement with the previous results (Fig. 4). S is increasing with the incorporation of ceramic powder and has smaller values in the case of large particle size (235, 266 and 315 cm^{-1} respectively for $d_{50} = 2.3$, 1.4 and 0.5 µm). That explained the increase of the diffuse reflectance and the decrease of diffuse transmittance (Fig. 2).

As the calculated absorptance, K is increasing up to a maximum value of ~80 cm^{-1} for a concentration of about 10 vol.% then is slightly decreasing for larger values of powder loading. The effect of the particle size on the variation of K is not obvious.

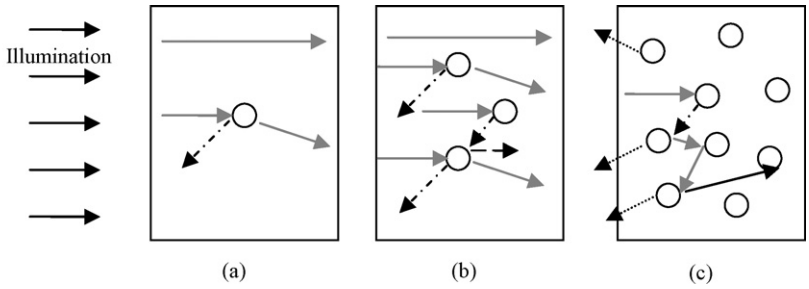

Fig. 3. Schematization of the variation of optical trajectories in ceramic suspensions at different powder loading.

The values of S (50–350 cm^{-1}) are largely higher than those of K (30–80 cm^{-1}), whatever the powder concentration, which suggest that the interaction of the UV-light with the alumina suspensions is controlled by the scattering, even for low concentrations (<10 vol.%).

3.3. Polymerization under a laser

The variations of the cure depth (C_D) and width (C_W), for powder concentrations ranging from 1 to 55 vol.% and for the three alumina powders, at $D_{Ei} = 156$ mJ/cm^2, are given in Fig. 5. Errors bars show the standard deviation for twenty independent polymerized features.

The C_D is decreasing as the concentration of the powder is increasing due to scattering (Fig. 5a). The effect of the mean particle size is not significant with variation included in the bars of errors. The small variation of C_D with the mean particle size seems curious as the optical properties of the three powders differ (T, R, K and S). Probably, our characterization procedure is not sensible enough to detect small variation of C_D.

The variation of C_W (Fig. 5b) presents a behavior close to absorptance (A_{cal}) and absorption coefficient K, but with a maximum obtained for a different powder concentration. Indeed, the C_W is increasing up to a about 3–5 vol.% alumina, then is decreasing to stabilize for a value of 340 μm beyond 30 vol.% powder. The threshold concentrations did not represent the same physical mechanisms in the variation of C_W and of absorption, and no deeper understanding is achieved at present.

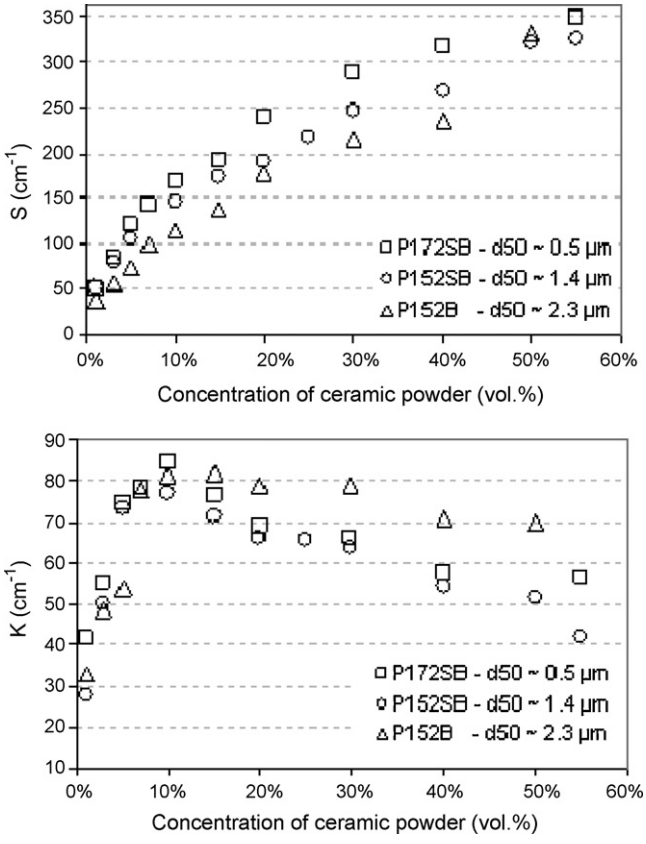

Fig. 4. Variation of S (a) and K (b) coefficients with the powder loading for the three alumina at $\lambda = 351$ nm.

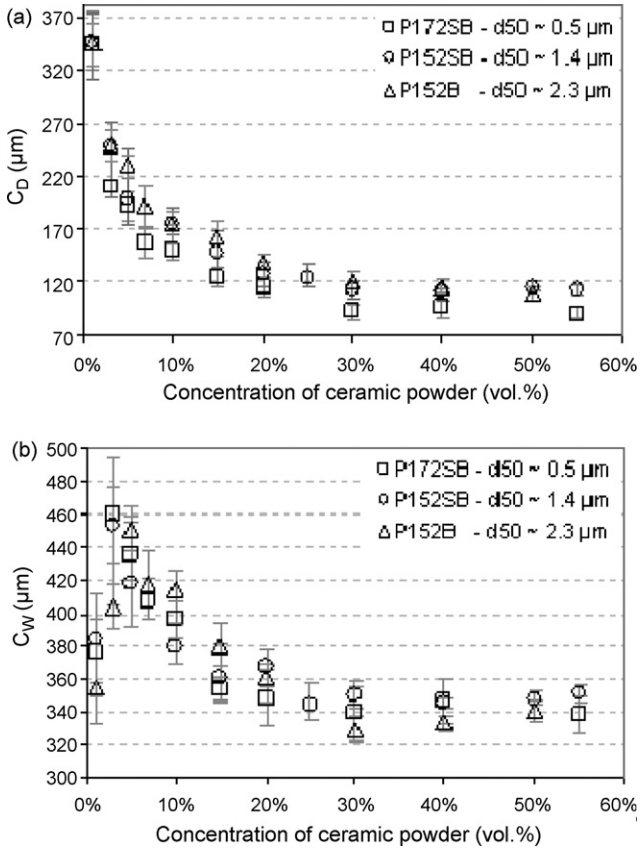

Fig. 5. Variations of C_D (a) and C_W (b) with the powder loading for the three alumina suspensions ($D_{Ei} = 156$ mJ/cm^2).

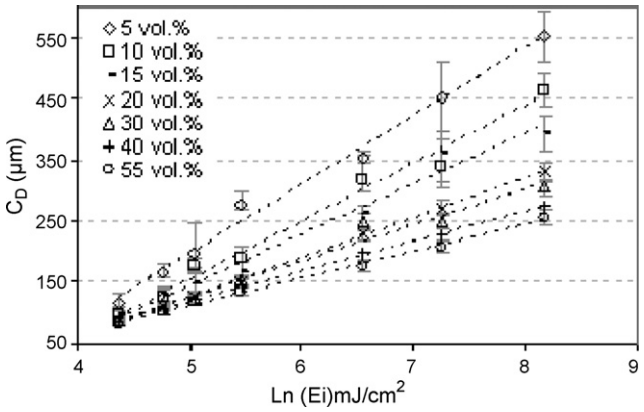

Fig. 6. Variation of C_D with ln(E_i) for P152SB alumina (d_{50} = 1.4 µm).

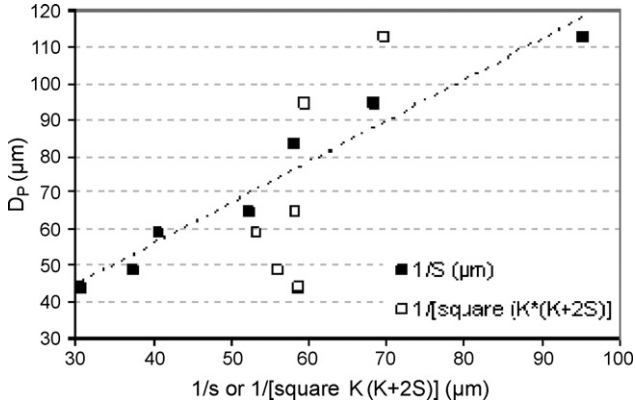

Fig. 7. Variation of D_p versus $1/S$ and $1/\sqrt{K(K+2S)}$ for the P152SB alumina (d_{50} = 1.4 µm).

As for C_D, no significant variation of C_W is observed with the particle size.

The variation of the C_D with density of energy (E_i = 78–3495 mJ/cm^2) for different concentr-ations of the three alumina were studied. The example of the P152SB alumina (d_{50} = 1.4 µm) is reported in Fig. 6.

For the three alumina powders, the Jacobs law (Eq. (3)) is verified and calculated D_p values are reported in Table 1.

The K-M model can be considered as Beer's law with the difference that the last one only considers absorption (α), whereas the K-M model takes into account both absorption (K) and scattering (S) with:

$$E \equiv E_i \exp\left(-\left(\sqrt{(K(K+2S)}\right)z\right) \quad (10)$$

In the case of a homogeneous medium (un-scattering system, i.e. S = 0), this expression corresponds to the classical Beer's absorption law (Eq. (1)) with $\alpha \equiv K$.

The combination of the Jacobs law and the K-M model, both derived from the Beer's law, suggests that D_p and $\sqrt{K(K+2S)}$ are related. However, we observed that only the coefficient S described D_p as shown in Fig. 7, meaning that the polymerized depth is only controlled by scattering.

The comparison of Jacobs law and of the K-M expression led us to conclude that $1/D_P = \sqrt{K(K+2S)}$ but this is in contradiction with experimental results which suggest $1/D_P = S$, see Fig. 7, a fact already reported in the literature.[23] The K-M model predicts the decrease of the intensity with depth (z). He does not tell anything about the repartition of the intensity in a plane of constant depth. The density in this plane is uniform only in the case of a source of infinite extent. On the contrary, a laser source is of a small extent and the light intensity is strong enough to provoke polymerization only at the vertical of the laser beam impact. Scattered light is inefficient in this respect. Ray tracing simulations[23] have indeed shown that the integrated intensity over the plane of depth z verifies the z-dependence predicted by the K-M model while the direct beam intensity decreases as exp($-Sz$).

This behavior was validated for the three alumina suspensions as shown in Fig. 8 with a linear variation of D_p in function of $1/S$ (Table 2). The lines do not cross the origin. Over-estimated values of D_p (~10 µm) are probably due to an over-estimation of the coefficient S. Indeed, we have to remind that measurements of the diffuse reflectance used for the K and S computation are not corrected (the contribution of the interfaces effects is included).

Using the linear relation between D_p and $1/S$, Eq. (3) can be rewritten as:

$$C_D \cong \frac{1}{S} \ln\left(\frac{E_i}{E_c}\right) \quad (11)$$

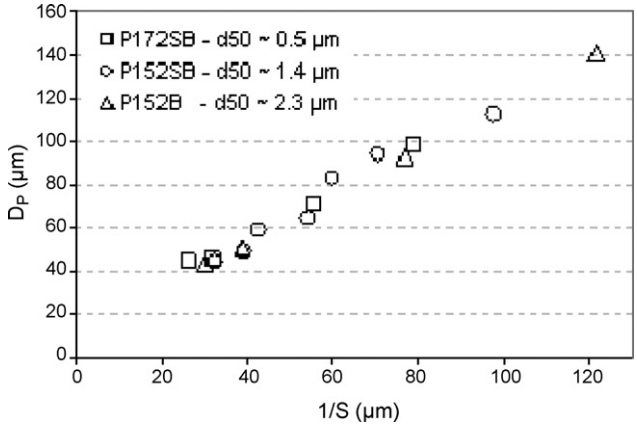

Fig. 8. Variation of D_p versus $1/S$ for the three alumina suspensions (P172SB – d_{50} = 0.5 µm; P152SB – d_{50} = 1.4 µm; P152 – d_{50} = 2.3 µm).

Table 1
D_p value of the three alumina suspensions.

Loading	5 vol.%	10 vol.%	15 vol.%	20 vol.%	30 vol.%	40 vol.%	50 vol.%	55 vol.%
D_p – P172SB (µm)	97.97	71.02	–	–	44.98	–	–	43.76
D_p – P152SB (µm)	112.54	94.18	83.07	64.48	58.92	48.80	–	43.75
D_p – P152 (µm)	141.14	92.66	–	–	50.51	–	43.62	–

Table 2
Linear relationship characteristics between D_p and $1/S$ for the three alumina suspensions.

	P172SB	P152SB	P152
Slope	1.026	1.119	0.958
Intercept*	11.66	11.02	10.21
R^2 statistic	0.993	0.954	0.993

* D_p at $1/S = 0$.

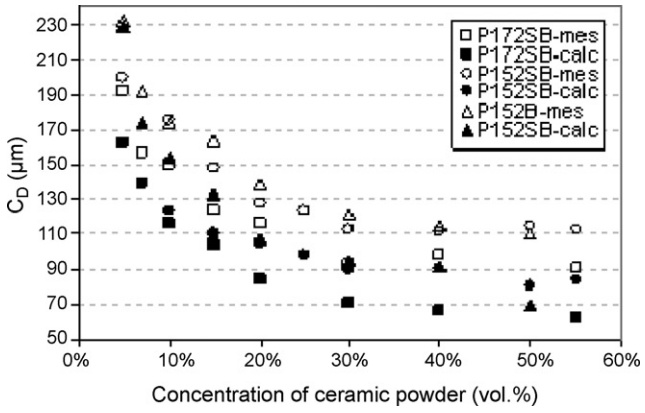

Fig. 9. Comparison between the measured (mes) and the predicted (calc) C_D for the three alumina suspensions (P172SB – $d_{50} = 0.5$ μm; P152SB – $d_{50} = 1.4$ μm; P152 – $d_{50} = 2.3$ μm).

This last expression makes it possible to predict C_D, with a rather good agreement, from simple measurements of diffuse reflectance as shown in Fig. 9. An under-valuation of about 20% is observed, which is due to the over-estimation of the factor S mentioned above.

4. Conclusion

The optical properties of the stereolithography alumina suspensions were studied using the UV diffuse reflectance and transmittance measurements following by the Kubelka–Munk analysis. The interaction of the UV light with alumina suspensions is governed by the scattering, even for low powder concentrations.

The increase of the particle size increases the transmission and decreases the reflectance. But no significant influence of the particle size on the cure depth and width was observed, likely due to the accuracy of our experimental procedure of measurement.

The scattering (S) was satisfactory related to the depth of penetration (D_p). A quantitative relationship between the cure depth (C_D) and (S) was proposed to predict C_D with an error of about 20% due an over-estimation of the factor S. This model will be applied to other ceramic materials in order to evaluate its validity and will be discussed in a forthcoming paper.

References

1. Hull, C., Apparatus for production of three-dimensional objects by stereolithography, U.S. Pat. No. 4575 330, 1986.
2. Griffith, M. L. and Halloran, J. W., Freeform fabrication of ceramics via stereolithography. *J. Am. Ceram. Soc.*, 1996, **79**(10), 2601–2608.
3. Griffith, M. L. and Halloran, J. W., Ultraviloet curable ceramic suspension for stereolithography of ceramics. *Manuf. Sci. Eng.*, 1994, **2**, 529–534.
4. Griffith, M. L. *et al.*, Ceramic stereolithography for investment casting and biomedical applications solid freeform fabrication. In *Conf. SFF'95*, 1995, pp. 31–38.
5. Griffith, M. L. and Halloran, J. W., Scattering of ultraviolet radiation in turbid suspensions. *J. Appl. phys.*, 1997, **81**(6), 2538–2546.
6. Liao, H. and Coyle, T. W., Photoactive suspensions for stereolithography of ceramics. *J. Can. Ceram. Soc.*, 1996, **65**(4), 254–262.
7. Hinczewski, C. *et al.*, Ceramic suspension suitable for stereolithography. *J. Eur. Ceram. Soc.*, 1998, **18**, 583–590.
8. Jang, J. H. *et al.*, Preparation and characterization of Barium Titanate Suspensions for stereolithography. *J. Am. Ceram. Soc.*, 2000, **83**(4), 1804–1806.
9. Greco, A. *et al.*, Stereolithography of ceramic suspensions. *J. Mater. Sci. Soc.*, 2001, **36**, 99–105.
10. Chartier, T. and Chaput, C., Stereolithography as a shaping technique for ceramics. *Bull. Eur. Ceram. Soc.*, 2003, **1**, 29–32.
11. Dufaud, O. *et al.*, Rheological properties of PZT suspensions for stereolithography. *J. Eur. Ceram. Soc.*, 2002, **22**(13), 2081–2092.
12. Licciulli, A. *et al.*, Laser stereolithography of ZrO2 toughened Al2O3. *J. Eur. Ceram. Soc.*, 2004, **24**(15–16), 3769–3777.
13. Wu, K. C. *et al.*, Prediction of ceramic stereolithography resin sensitivity from theory and measurement of diffusive photon transport. *J. Appl. Phys.*, 2005, **98**(2), 24902–24912.
14. Hinczewski, C., Stéréolithographie pour la fabrication de ceramiques, Ph.D. Thesis, ENSIC, Nancy, 1998.
15. Kubelka, P. and Munk, F., New contributions to the optics of intensely light-scattering materials – part I. *J. Opt. Soc. Am.*, 1948, **38**, 448–457.
16. Kubelka, P., New contributions to the optics of intensely light-scattering materials – part II. Non-homogeneous layers. *J. Opt. Soc. Am.*, 1954, **44**(4), 330–335.
17. Kubelka, P. and Munk, F., Ein Beitrag zur Optik der Far-banstriche. *Zeits. F. techn. Physik*, 1931, **12**, 593–601.
18. Saunderson, J. L., Calculation of the color of pigmented plastics. *J. Opt. Soc. Am.*, 1942, **32**, 727–736.
19. Cook, W. D. and McAree, D. C., Optical properties of esthetic restorative materials and natural dentition. *J. Biomed. Mater. Res.*, 1985, **19**, 469–488.
20. Taira, M. and Yamaki, M., Studies on optical properties of a visible-light-cured dental composite resin by diffuse reflectance measurements. *J. Mate. Sci. Lett.*, 1995, **14**, 198–200.
21. Bondioli, F. *et al.*, Color matching algorithms in ceramic tile production. *J. Eur. Ceram. Soci.*, 2006, **26**(3), 311–316.
22. Chirdon, W. M. *et al.*, Diffuse reflectance of short-fiber-reinforced composites aligned by an electric field. *Dent. Mater.*, 2006, **22**(1), 57–62.
23. Faure, S., Etude de l'interaction rayonnement- matière dans un milieu granulaire en vue de l'application au procédé de frittage laser, Ph.D. Thesis, ENSCI, Limoges, 2004.